

Ground-state properties of a Peierls-Hubbard triangular prism

Shoji Yamamoto¹, Jun Ohara² and Masa-aki Ozaki³

¹*Department of Physics, Hokkaido University, Sapporo 060-0810, Japan*

²*Division of Physics, Yokohama National University, Yokohama 240-8501, Japan and*

³*Uji 611-0002, Japan*

(Dated: 17 December 2009)

Motivated by recent chemical attempts at assembling halogen-bridged transition-metal complexes within a nanotube, we model and characterize a platinum-halide triangular prism in terms of a Peierls-Hubbard Hamiltonian. Based on a group-theoretical argument, we reveal a variety of valence arrangements, including heterogeneous or partially metallic charge-density-wave states. Quantum and thermal phase competitions are numerically demonstrated with particular emphasis on novel insulator-to-metal and insulator-to-insulator transitions under doping, the former of which is of the first order, while the latter of which is of the second order.

PACS numbers: 71.10.Hf, 71.45.Lr, 02.20.-a, 78.20.Bh

I. INTRODUCTION

The success of patterning a graphite sheet into a cylinder¹⁻³ stimulated the public interest in the geometric tunability of electronic properties. Carbon nanotubes indeed vary from metals to semiconductors with the inside diameter and the chiral angle.⁴ Their nature is fairly describable within the π -electron nearest-neighbor tight-binding model^{5,6} and is relatively insensitive to Coulomb interactions. A tubed vanadium oxide,⁷ $\text{Na}_2\text{V}_3\text{O}_7$, consists of strongly correlated d electrons, but they are completely localized. Another transition-metal-based nanotubular compound,⁸ $[\text{Cl}(\text{CuCl}_2\text{tachH})_3]\text{X}_2$ ($\text{X} = \text{Cl}, \text{Br}$; tach = *cis, trans*-1, 3, 5-triamino-cyclohexane = $\text{C}_{18}\text{H}_{45}\text{N}_9$), also behaves as a Heisenberg magnet. In such circumstances, a platinum-iodide quadratic-prism compound,⁹ $[\text{Pt}(\text{en})(\text{bpy})\text{I}]_4(\text{NO}_3)_8$ (en = ethylenediamine = $\text{C}_2\text{H}_8\text{N}_2$; bpy = 4, 4'-bipyridyl = $\text{C}_{10}\text{H}_8\text{N}_2$), featured by competing electron-electron and electron-lattice interactions, has sparked a brandnew interest¹⁰ in lattice electron nanostructures.

Quasi-one-dimensional transition-metal (M) complexes with bridging halogens (X) possess unique optoelectronic properties,¹¹⁻¹⁴ which are widely variable according to the constituent metals, halogens, ligand molecules and counter ions.¹⁵ Platinum-halide single-chain compounds such as Wolfram's red salt¹⁶ $[\text{Pt}(\text{ea})_4\text{Cl}]\text{Cl}_2 \cdot 2\text{H}_2\text{O}$ (ea = ethylamine = $\text{C}_2\text{H}_7\text{N}$) have a Peierls-distorted mixed-valent ground state, whereas their nickel analogs^{17,18} consist of Mott-insulating monovalent regular chains. In between are palladium halides, whose ground states can be tuned optically^{19,20} and electrochemically.^{21,22} Metal binucleation considerably stimulates the electronic activity.^{23,24} A diplatinum-iodide chain compound,²⁵ $R_4[\text{Pt}_2(\text{pop})_4\text{I}]$ [pop = diphosphonate = $\text{P}_2\text{O}_5\text{H}_2$; $R = (\text{C}_2\text{H}_5)_2\text{NH}_2$], exhibits photo- and pressure-induced phase transitions,²⁶⁻³⁰ while its analog without any counter ion,³¹ $\text{Pt}_2(\text{dta})_4\text{I}$ (dta = dithioacetate = CH_3CS_2), is of metallic conduction at room temperature and undergoes a double

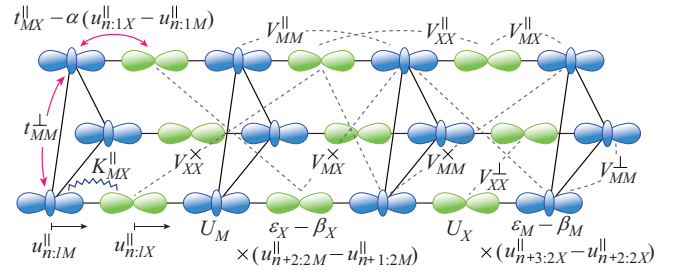


FIG. 1: (Color online) Modeling of an MX triangular prism, where heavily and lightly shaded clouds denote $M d_{z^2}$ and $X p_z$ orbitals, the electron numbers on which are calculated through $n_{n:1Ms} \equiv a_{n:1Ms}^\dagger a_{n:1Ms}$ and $n_{n:1Xs} \equiv a_{n:1Xs}^\dagger a_{n:1Xs}$, respectively. The on-site energies (electron affinities) of isolated atoms are given by ε_M and ε_X , while the electron hops between these levels are expressed by t_{MX}^{\parallel} and t_{MM}^{\parallel} . The on-site Coulomb interactions are labeled as U_A ($A = M, X$), whereas the interchain and intrachain different-site Coulomb interactions as $V_{AA'}^{\perp}$, $V_{AA'}^x$ and $V_{AA'}^{\parallel}$ ($A, A' = M, X$). The leg-direction displacements of metal and halogen ions, $u_{n:1M}^{\parallel}$ and $u_{n:1X}^{\parallel}$, interact with electrons through the intersite (α) and intrasite (β_M, β_X) coupling constants at the cost of elastic energy due to the spring constant K_{MX}^{\parallel} .

transition to a novel Peierls insulator with decreasing temperature.^{32,33} $(\mu\text{-bpym})[\text{Pt}(\text{en})\text{X}]_2\text{X}(\text{ClO}_4)_3 \cdot \text{H}_2\text{O}$ ($\text{X} = \text{Cl}, \text{Br}$; $\mu\text{-bpym} = 2, 2'$ -bipyrimidine = $\text{C}_8\text{H}_6\text{N}_4$)³⁴ and $(\text{bpy})[\text{Pt}(\text{dien})\text{Br}]_2\text{Br}_4 \cdot 2\text{H}_2\text{O}$ (dien = diethylenetriamine = $\text{C}_4\text{H}_{13}\text{N}_3$)³⁵ were synthesized in an attempt to bring a couple of MX chains into interaction. They are made in similar ladder structures but in distinct ground states of mixed valence,^{36,37} which are optically distinguishable.^{38,39}

Thus and thus, the MX class of materials have been fascinating numerous chemists and physicists for more than half a century. Much effort is still devoted to elaborating new varieties and the novel porous nanotube $[\text{Pt}(\text{en})(\text{bpy})\text{I}]_4(\text{NO}_3)_8$ has just been fabricated. Diffuse X-ray scattering measurements⁹ on it suggest two or more cell-doubled mixed-valent phases compet-

ing with each other in the ground state. Such phases are indeed recognizable as broken-symmetry solutions of a four-legged Peierls-Hubbard Hamiltonian of tetragonal symmetry.¹⁰ Then we may have an idea of bringing coupled MX chains into geometric frustration. A platinum-halide triangular-prism compound must be a unique charge-frustrated nanotubular system and may exhibit novel valence arrangements which have never been observed in any other material. Thus motivated, we apply a group-theoretical bifurcation theory^{40,41} to a three-legged Peierls-Hubbard Hamiltonian of hexagonal symmetry and reveal its exotic ground states. They are numerically calculated and compared with each other in an attempt to guide future experiments.

II. MODEL HAMILTONIAN AND ITS SYMMETRY PROPERTIES

Metal-halide triangular prisms are describable in terms of a two-band extended Peierls-Hubbard Hamiltonian of hexagonal symmetry,

$$\begin{aligned}
\mathcal{H} = & \sum_{l,n,s} \left\{ [t_{MX}^{\parallel} - \alpha(u_{n+1:lM}^{\parallel} - u_{n:lX}^{\parallel})] a_{n+1:lMs}^{\dagger} a_{n:lXs} \right. \\
& - [t_{MX}^{\parallel} - \alpha(u_{n:lX}^{\parallel} - u_{n:lM}^{\parallel})] a_{n:lXs}^{\dagger} a_{n:lMs} \\
& \left. - t_{MM}^{\perp} a_{n:l+1Ms}^{\dagger} a_{n:lMs} + \text{H.c.} \right\} \\
& + \sum_{l,n,s} \left\{ [\varepsilon_M - \beta_M(u_{n:lX}^{\parallel} - u_{n-1:lX}^{\parallel})] n_{n:lMs} \right. \\
& \left. + [\varepsilon_X - \beta_X(u_{n+1:lM}^{\parallel} - u_{n:lM}^{\parallel})] n_{n:lXs} \right\} \\
& + \sum_{l,n} \frac{K_{MX}^{\parallel}}{2} [(u_{n:lX}^{\parallel} - u_{n:lM}^{\parallel})^2 + (u_{n+1:lM}^{\parallel} - u_{n:lX}^{\parallel})^2] \\
& + \sum_{A=M,X} \sum_{l,n,s,s'} \left\{ \frac{U_A}{4} n_{n:lAs} n_{n:lA-s} + V_{AA}^{\parallel} n_{n:lAs} n_{n+1:lAs'} \right. \\
& + V_{AA}^{\times} (n_{n:lAs} n_{n+1:l+1As'} + n_{n:l+1As} n_{n+1:lAs'}) \\
& \left. + V_{AA}^{\perp} n_{n:lAs} n_{n:l+1As'} \right\} \\
& + \sum_{l,n,s,s'} \left\{ V_{MX}^{\parallel} (n_{n:lMs} n_{n:lXs'} + n_{n:lXs} n_{n+1:lMs'}) \right. \\
& + V_{MX}^{\times} (n_{n:lMs} n_{n:l+1Xs'} + n_{n:l+1Ms} n_{n:lXs'}) \\
& \left. + n_{n:lXs} n_{n+1:l+1Ms'} + n_{n:l+1Xs} n_{n+1:lMs'} \right\}, \quad (2.1)
\end{aligned}$$

where MX chain legs and M_3X_3 prism units are numbered by $l = 1, 2, 3$ and $n = 1, 2, \dots, N$, respectively, while electron spins are indicated by $s, s' = \uparrow, \downarrow$. The modeling is visualized and explained in more detail in Fig. 1.

Unless the gauge symmetry is broken, the symmetry group of any lattice electron system can be written as $\mathbf{G} = \mathbf{P} \times \mathbf{S} \times \mathbf{T}$, where \mathbf{P} , \mathbf{S} and \mathbf{T} are the groups of space, spin rotation, and time reversal, respectively. The space group is further decomposed into

the translation and point groups as $\mathbf{L} \wedge \mathbf{D}$. For $M d_{z^2} - X p_z$ triangular prisms, \mathbf{L} and \mathbf{D} read as $\{\mathbf{E}, l\} \equiv \mathbf{L}_1$ and \mathbf{D}_{3h} , respectively, where l is the unit-cell translation in the z direction. Defining the Fourier transformation as $a_{k:lAs} = N^{-1/2} \sum_n e^{-ik(n+\delta_{AX}/2)} a_{n:lAs}$ and $u_{k:lA}^{\parallel} = N^{-1/2} \sum_n e^{-ik(n+\delta_{AX}/2)} u_{n:lA}^{\parallel}$ with the lattice constant along the tube axis set equal to unity and composing Hermitian bases of the gauge-invariant operators $\{a_{k:lAs}^{\dagger} a_{k':l'A's'}\}$, we find out irreducible representations of \mathbf{G} over the real number field, which are referred to as $\check{\mathbf{G}}$. Actions of $l \in \mathbf{L}_1$ and $t \in \mathbf{T}$ on the electron operators are defined as $l \cdot a_{k:lAs}^{\dagger} = e^{-ikl} a_{k:lAs}^{\dagger}$ and $t \cdot a_{k:lAs}^{\dagger} = (-1)^{\delta_{s\uparrow}} a_{-k:lA-s}^{\dagger}$. Those of $p \in \mathbf{D}_{3h}$ are calculated as $p \cdot a_{k:lMs}^{\dagger} = [A'_1(p)]_{11} a_{pk:lMs}^{\dagger}$ and $p \cdot a_{k:lXs}^{\dagger} = [A''_2(p)]_{11} a_{pk:lXs}^{\dagger}$, where $[\check{D}(p)]_{ij}$ is the (i, j) -element of the \check{D} representation matrix for p . Those of $u(\mathbf{e}, \theta) = \sigma^0 \cos(\theta/2) - i(\boldsymbol{\sigma} \cdot \mathbf{e}) \sin(\theta/2) \in \mathbf{S}$ are represented as $u(\mathbf{e}, \theta) \cdot a_{k:lAs}^{\dagger} = \sum_{s'} [u(\mathbf{e}, \theta)]_{s's} a_{k:lAs'}^{\dagger}$, where σ^0 and $\boldsymbol{\sigma} = (\sigma^x, \sigma^y, \sigma^z)$ are the 2×2 unit matrix and a vector composed of the Pauli matrices, respectively. Any representation \check{G} is expressed as $\check{G} = \check{P} \otimes \check{S} \otimes \check{T}$. Once a wave vector Q is fixed, the relevant little group $\mathbf{D}(Q)$ is given. \check{P} is therefore labeled as $Q\check{D}(Q)$. The relevant representations of \mathbf{S} are given by $\check{S}^0(u(\mathbf{e}, \theta)) = 1$ (singlet) and $\check{S}^1(u(\mathbf{e}, \theta)) = O(u(\mathbf{e}, \theta))$ (triplet), where $O(u(\mathbf{e}, \theta))$ is the 3×3 orthogonal matrix satisfying $u(\mathbf{e}, \theta) \boldsymbol{\sigma}^{\lambda} u^{\dagger}(\mathbf{e}, \theta) = \sum_{\mu=x,y,z} [O(u(\mathbf{e}, \theta))]_{\lambda\mu} \boldsymbol{\sigma}^{\mu}$ ($\lambda = x, y, z$). Those of \mathbf{T} are given by $\check{T}^0(t) = 1$ (symmetric) and $\check{T}^1(t) = -1$ (antisymmetric). Considering that platinum $5d$ electrons are moderately correlated, magnetically broken-symmetry solutions are less interesting. Nontrivial current-wave phases, whether of charge⁴² or of spin,⁴³ are of little occurrence unless electrons are well itinerant in both leg and rung directions. Therefore, we discuss density-wave solutions of the $\check{P} \otimes \check{S}^0 \otimes \check{T}^0$ type. Since the relevant d_{z^2} and p_z orbitals of constituent MX chains are formally half and fully filled, respectively, we take much interest in cell-doubled mixed-valent states among others. Increasing temperature and/or electrochemical doping may suppress lattice dimerization and induce valence delocalization. Thus we consider the cases of $Q = 0$ and $Q = \pi$, which are described by the translation groups $\mathbf{L}_1 \equiv \{\mathbf{E}, l\}$ and $\mathbf{L}_2 \equiv \{\mathbf{E}, 2l\}$, respectively, and are hereafter referred to as Γ and X , respectively. Both $\mathbf{D}(\Gamma)$ and $\mathbf{D}(X)$ read as \mathbf{D}_{3h} .

We take the Hartree-Fock scheme of rewriting the Hamiltonian (2.1) into

$$\begin{aligned}
\mathcal{H}_{\text{HF}} = & \sum_{l,l'} \sum_{A,A'} \sum_{Q=\Gamma,X} \sum_{k,s,s'} \sum_{\lambda=0,x,y,z} x_{lAl'A'}^{\lambda}(Q; k) \\
& \times a_{k+Q:lAs}^{\dagger} a_{k:l'A's'} \sigma_{ss'}^{\lambda} \equiv \sum_Q \sum_{\lambda} h_Q^{\lambda}, \quad (2.2)
\end{aligned}$$

where the self-consistent fields $x_{lAl'A'}^{\lambda}(Q; k)$, as well as the lattice distortions $u_{Q:lA}^{\parallel}$, can be described in terms of the density matrices $\rho_{l'A'lA}^{\lambda}(Q; k) =$

TABLE I: Symmetry properties of irreducible representations, $\Gamma\check{D}(\Gamma) \otimes \check{S}^0 \otimes \check{T}^0$ and $X\check{D}(X) \otimes \check{S}^0 \otimes \check{T}^0$, available on the condition of axial isotropy subgroup.

Irreducible representation	Axial isotropy subgroup	Fixed-point subspace	Broken-symmetry Hamiltonian	Physical character
$\Gamma A'_1 \otimes \check{S}^0 \otimes \check{T}^0$	$\mathbf{D}_{3h}\mathbf{L}_1\mathbf{ST}$	$h_{\Gamma A'_1[1,1]}^{00}$	$h_{\Gamma A'_1[1,1]}^{00}$	PM
$\Gamma A'_2 \otimes \check{S}^0 \otimes \check{T}^0$	$\mathbf{C}_{3h}\mathbf{L}_1\mathbf{ST}$	$h_{\Gamma A'_2[1,1]}^{00}$	$h_{\Gamma A'_2[1,1]}^{00} + h_{\Gamma A'_1[1,1]}^{00}$	\vee -MX-BOW
$\Gamma A''_1 \otimes \check{S}^0 \otimes \check{T}^0$	$\mathbf{D}_3\mathbf{L}_1\mathbf{ST}$	$h_{\Gamma A''_1[1,1]}^{00}$	$h_{\Gamma A''_1[1,1]}^{00} + h_{\Gamma A'_1[1,1]}^{00}$	$\backslash\backslash$ -MX-BOW
$\Gamma A'_2 \otimes \check{S}^0 \otimes \check{T}^0$	$\mathbf{C}_{3v}\mathbf{L}_1\mathbf{ST}$	$h_{\Gamma A'_2[1,1]}^{00}$	$h_{\Gamma A'_2[1,1]}^{00} + h_{\Gamma A'_1[1,1]}^{00}$	$(- - -)$ -MX-BOW
$\Gamma E'(1) \otimes \check{S}^0 \otimes \check{T}^0$	$\mathbf{C}_{2v}\mathbf{L}_1\mathbf{ST}$	$h_{\Gamma E'[1,1]}^{00}$	$h_{\Gamma E'[1,1]}^{00} + h_{\Gamma A'_1[1,1]}^{00}$	Δ -MM-BOW
$\Gamma E''(1) \otimes \check{S}^0 \otimes \check{T}^0$	$(1 + \sigma_{v1})\mathbf{L}_1\mathbf{ST}$	$h_{\Gamma E''[1,1]}^{00}$	$h_{\Gamma E''[1,1]}^{00} + h_{\Gamma A'_2[1,1]}^{00} + h_{\Gamma E'[1,1]}^{00} + h_{\Gamma A'_1[1,1]}^{00}$	$(\pm - -)$ -MX-BOW
$\Gamma E''(2) \otimes \check{S}^0 \otimes \check{T}^0$	$(1 + C'_{21})\mathbf{L}_1\mathbf{ST}$	$h_{\Gamma E''[2,2]}^{00}$	$h_{\Gamma E''[2,2]}^{00} + h_{\Gamma A'_1[1,1]}^{00} + h_{\Gamma E'[1,1]}^{00} + h_{\Gamma A'_1[1,1]}^{00}$	$(0 - +)$ -MX-BOW
$XA'_1 \otimes \check{S}^0 \otimes \check{T}^0$	$\mathbf{D}_{3h}\mathbf{L}_2\mathbf{ST}$	$h_{XA'_1[1,1]}^{00}$	$h_{XA'_1[1,1]}^{00} + h_{\Gamma A'_1[1,1]}^{00}$	$(+ + +)$ -M-CDW
$XA'_2 \otimes \check{S}^0 \otimes \check{T}^0$	$(1 + C'_{21})\mathbf{C}_{3h}\mathbf{L}_2\mathbf{ST}$	$h_{XA'_2[1,1]}^{00}$	$h_{XA'_2[1,1]}^{00} + h_{\Gamma A'_1[1,1]}^{00}$	\times -MM-BOW
$XA'_1 \otimes \check{S}^0 \otimes \check{T}^0$	$(1 + \sigma_h)\mathbf{D}_3\mathbf{L}_2\mathbf{ST}$	$h_{XA'_1[1,1]}^{00}$	$h_{XA'_1[1,1]}^{00} + h_{\Gamma A'_1[1,1]}^{00}$	\times -XX-BOW
$XA'_2 \otimes \check{S}^0 \otimes \check{T}^0$	$(1 + C'_{21})\mathbf{C}_{3v}\mathbf{L}_2\mathbf{ST}$	$h_{XA'_2[1,1]}^{00}$	$h_{XA'_2[1,1]}^{00} + h_{\Gamma A'_1[1,1]}^{00}$	$(+ + +)$ -X-CDW
$XE'(1) \otimes \check{S}^0 \otimes \check{T}^0$	$\mathbf{C}_{2v}\mathbf{L}_2\mathbf{ST}$	$h_{XE'[1,1]}^{00}$	$h_{XE'[1,1]}^{00} + h_{XA'_1[1,1]}^{00} + h_{\Gamma E'[1,1]}^{00} + h_{\Gamma A'_1[1,1]}^{00}$	$(\pm + +)$ -M-CDW
$XE'(2) \otimes \check{S}^0 \otimes \check{T}^0$	$(1 + C'_{21})\mathbf{C}_{1h}\mathbf{L}_2\mathbf{ST}$	$h_{XE'[2,2]}^{00}$	$h_{XE'[2,2]}^{00} + h_{XA'_2[1,1]}^{00} + h_{\Gamma E'[1,1]}^{00} + h_{\Gamma A'_1[1,1]}^{00}$	$(0 + -)$ -M-CDW
$XE''(1) \otimes \check{S}^0 \otimes \check{T}^0$	$(1 + C'_{21})\mathbf{L}_2\mathbf{ST}$	$h_{XE''[1,1]}^{00}$	$h_{XE''[1,1]}^{00} + h_{XA'_2[1,1]}^{00} + h_{\Gamma E'[1,1]}^{00} + h_{\Gamma A'_1[1,1]}^{00}$	$(\pm + +)$ -X-CDW
$XE''(2) \otimes \check{S}^0 \otimes \check{T}^0$	$(1 + C'_{21})(1 + \sigma_{v1})\mathbf{L}_2\mathbf{ST}$	$h_{XE''[2,2]}^{00}$	$h_{XE''[2,2]}^{00} + h_{XA'_1[1,1]}^{00} + h_{\Gamma E'[1,1]}^{00} + h_{\Gamma A'_1[1,1]}^{00}$	$(0 + -)$ -X-CDW

$\sum_{s,s'} \langle a_{k+Q;lAs}^\dagger a_{k:l'A's'} \rangle_T \sigma_{ss'}^\lambda / 2$ with $\langle \dots \rangle_T$ denoting the canonical average and are adiabatically determined at each temperature T so as to minimize the free energy. Employing the projection operators

$$P_{\check{D}[i,j]}^\tau = \frac{d_{\check{D}}}{2g} \sum_{t \in \mathbf{T}} \check{T}^\tau(t) \sum_{p \in \mathbf{D}_{3h}} [\check{D}(p)]_{ij}^* t p, \quad (2.3)$$

where $g (= 12)$ is the order of \mathbf{D}_{3h} and $d_{\check{D}} (\leq 2)$ is the dimension of its arbitrary irreducible representation \check{D} , we further decompose the Hamiltonian (2.2) into its fixed-point subspaces as

$$\mathcal{H}_{\text{HF}} = \sum_{Q=\Gamma,X} \sum_{\check{D}(Q)} \sum_{\lambda=0,x,y,z} \sum_{\tau=0,1} h_{Q\check{D}(Q)}^{\lambda\tau}, \quad (2.4)$$

where $h_{Q\check{D}[i,j]}^{\lambda\tau} = P_{\check{D}[i,j]}^\tau \cdot h_Q^\lambda$. We list in Table I the thus-obtained irreducible representations together with their broken-symmetry Hamiltonians. The two-dimensional representations E' and E'' are generally available in a variety of isotropy subgroups. Here we consider only the axial ones discarding those of two-dimensional fixed point subspace. Every irreducible representation is guaranteed to yield a stable solution only when its isotropy subgroup possesses a one-dimensional fixed point subspace.⁴⁴ Considering that the density matrices are of the same symmetry as their host Hamiltonian, we learn the oscillating pattern of electron densities, $\sum_s \langle a_{n;lAs}^\dagger a_{n;lAs} \rangle_T \equiv d_{n;lA}$, and bond orders, $\text{Re} \sum_s \langle a_{n;lAs}^\dagger a_{n';l'A's'} \rangle_T \equiv p_{n;lA;n':l'A'}$. In Fig. 2 we draw and name the consequent charge-density-wave (CDW) solutions, including bond-order-wave (BOW) ones which are recognizable as bond-centered CDW states.

Two kinds of axial isotropy subgroups are available from all the two-dimensional representations but $\Gamma E'$. A single state is derived from each of the second kind, whereas two quantitatively different states can be born to each of the first kind, which are distinguishably nicknamed. These symmetrically (qualitatively) degenerate but practically (quantitatively) distinct varieties read as heterogeneous CDW states, where each chain is no longer 3/4-filled, that is, one or two chains are charge-rich, while the rest are charge-poor. Such an interchain charge polarization is common to all the two-dimensional representations, including $\Gamma E'(1) \otimes \check{S}^0 \otimes \check{T}^0$. The thus-broken electron-hole symmetry yields an exotic phase diagram. It is the geometric frustration rather than any orbital hybridization that breaks down the electron-hole symmetry in triangular-prism MX complexes. It is not the case with even-legged ladders³⁸ and prisms,¹⁰ where the electron-hole symmetry is kept within any single-band description and the d -electron phase diagram as a function of doping is symmetric with respect to the half occupancy.

All the $\Gamma\check{D}(\Gamma) \otimes \check{S}^0 \otimes \check{T}^0$ solutions but the paramagnetic metal (PM) of the full symmetry $\mathbf{D}_{3h}\mathbf{L}_1\mathbf{ST}$ are characterized as BOW states. There is no lattice distortion in some of them under the present modeling, but even Δ -MM-BOW may be accompanied by cell deformation on the assumption that the interchain electron transfer t_{MM}^\perp can be coupled to phonons. Every BOW may be stabilized by electrons directly hopping on the oscillating bonds and their interactions with phonons, but any is of little occurrence within realistic modeling and parametrization. BOW states are more likely to appear

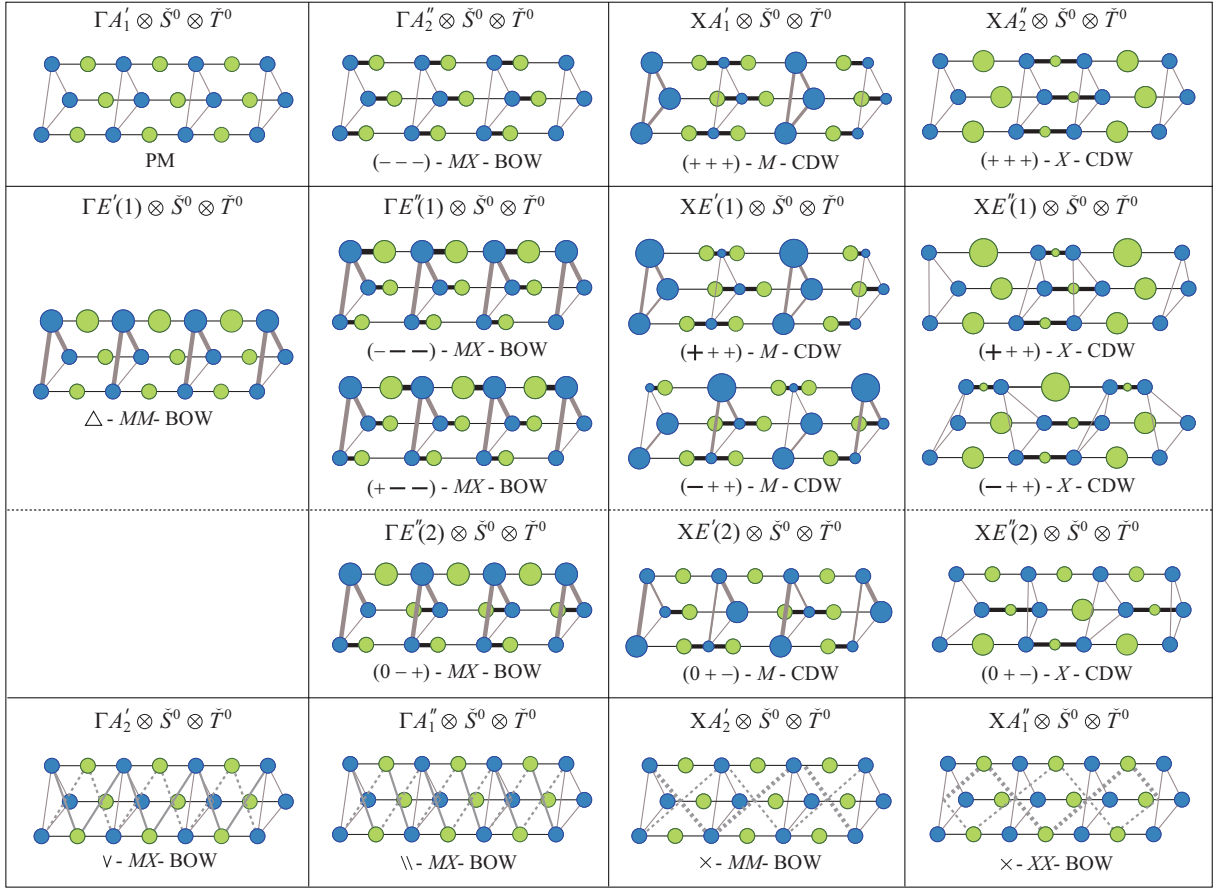


FIG. 2: (Color online) Charge-density-wave (CDW) and bond-order-wave (BOW) states obtained from the irreducible representations listed in Table I, where varied circles and segments represent oscillating electron densities and bond orders, respectively, while irregularly arranged circles denote lattice distortion. Various M (X)-CDW states are referred to as $(\sigma_1, \sigma_2, \sigma_3)$, which signify the electron densities on adjacent metal (halogen) sites forming a triangular section of the prism and are measured in comparison with the average occupancy of each chain l . Some of BOW states are similarly nicknamed, where the signatures denote the length changes from the equidistant spacing of adjacent MX bonds forming a prism fragment. Coexistent normal (\pm) and larger accentuated (\pm) signatures represent quantitatively different amplitudes.

in decoupled chains of the MX ^{45,46} and MMX ^{27,33} types.

The $X\tilde{D}(X) \otimes \tilde{S}^0 \otimes \tilde{T}^0$ solutions are classified into three groups: CDWs on the metal sublattice with the halogen sublattice dimerized, those on the halogen sublattice with the metal sublattice dimerized and BOWs without any charge oscillation. We find twice three irreducible representations assuming a CDW character. There is a one-to-one correspondence between M - and X -CDWs. X -CDW states consist of mixed-valent halogen ions. p electrons may be activated with increasing ε_X and U_X , but platinum-fluorides are hard to fabricate. Although all CDW states gain a condensation energy due to the Peierls distortion, they are not necessarily gapped. Those of the $(0 + -)$ type are *partially metallic*, where only two chains are valence-trapped and the rest is valence-delocalized. Such states as cell-doubled but gapless at the Fermi level are never available from MX ladders³⁶ but generally possible in MX tubes, whose little groups $\mathbf{D}(X)$ necessarily have a two-dimensional irreducible representation of axial isotropy subgroup. All other CDW

states are fully gapped at the boundaries of the reduced Brillouin zone.

III. QUANTUM AND THERMAL PHASE DIAGRAMS

Now we numerically draw various phase diagrams. We model a trial MX prism on the platinum-halide ladder compound $(\mu\text{-bpym})[\text{Pt}(\text{en})X]_2X(\text{ClO}_4)_3 \cdot \text{H}_2\text{O}$.³⁴ Assuming that platinum ions are equally spaced in the leg and rung directions, $r_{MM}^{\parallel} = 2r_{MX}^{\parallel} = r_{MM}^{\perp}$, we set the transfer integrals for $t_{MM}^{\perp} = 0.4t_{MX}^{\parallel}$. The on-site electronic parameters are taken as $U_M = 0.80t_{MX}^{\parallel}$, $U_X = 0.66t_{MX}^{\parallel}$ and $\varepsilon_M - \varepsilon_X = 2.0t_{MX}^{\parallel}$, while the elastic constants are adjusted to $\alpha = 0.24\sqrt{t_{MX}^{\parallel}K_{MX}^{\parallel}}$ and $\beta_M = \beta_X = 0.65\sqrt{t_{MX}^{\parallel}K_{MX}^{\parallel}}$. Coulomb interactions between different sites are designed as $V_{MX}^{\parallel} = (U_M + U_X)/4$,

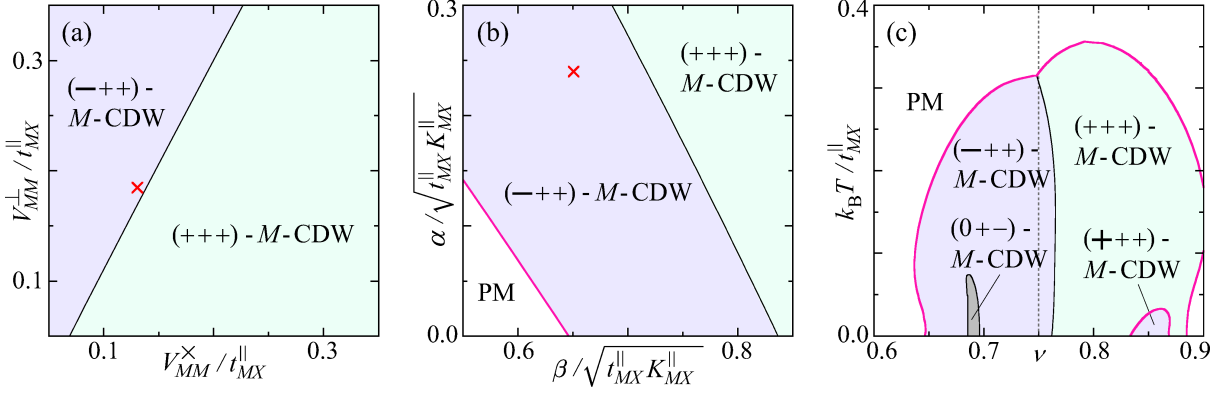


FIG. 3: (Color online) (a) A ground-state phase diagram with competing electron-electron interactions, V_{MM}^{\times} and V_{MM}^{\perp} ; (b) A ground-state phase diagram with varying electron-lattice couplings, α and $\beta \equiv \beta_M = \beta_X$; (c) A thermal phase diagram as a function of the electron occupancy ν , where the dotted line of $\nu = 3/4$ is a guide for eyes, separating the hole- and electron-doped regions. In all the diagrams the crosses indicate the standard parametrization stated in the text and we move away from this point tuning only the parameters in issue. Phase boundaries drawn in black and colored red (or toned down in monochromes) denote transitions of the first and second order, respectively.

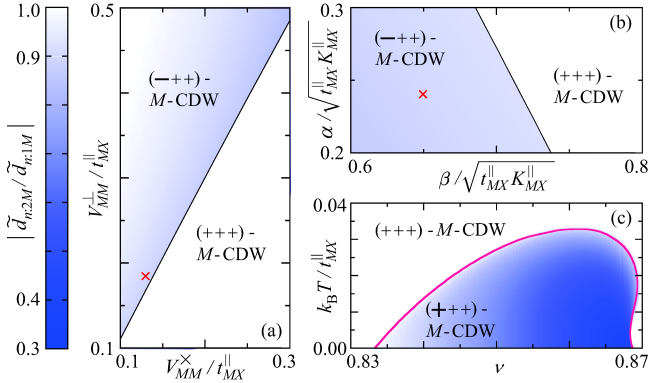


FIG. 4: (Color online) Contour plots of the ratio between the CDW amplitudes in the first and second chains on Figs. 3(a), 3(b) and 3(c) magnified.

$V_{AA}^{\parallel} = V_{MX}^{\parallel} r_{MX}^{\parallel} / r_{AA}^{\parallel}$, $V_{AA}^{\perp} = V_{MX}^{\parallel} r_{MX}^{\parallel} / r_{AA}^{\perp}$ and $V_{AA'}^{\times} = V_{MX}^{\parallel} r_{MX}^{\parallel} / \sqrt{(r_{MM}^{\perp})^2 + (r_{AA'}^{\parallel})^2}$. Such a parametrization is so realistic as to successfully interpret optical observations of existent platinum-halide two-leg ladders³⁸ and quadratic prisms.¹⁰ We employ these parameters unless otherwise noted, which are referred to as the standard parametrization and are indicated by \times in ground-state phase diagrams.

Figure 3 shows quantum and thermal phase competitions under varying electron-electron interactions, electron-lattice couplings and electron occupancy. Ground-state phase diagrams are calculated at a sufficiently low temperature, $k_B T / t_{MX}^{\parallel} = 0.001$. In $(-++)$ -M-CDW and $(++++)$ -M-CDW, three chains may unequally be distorted, that is, the CDW amplitude of one chain may be larger than those of the rest two. In order to detect such a heterogeneous CDW, we decompose the electron densities $d_{n:lM}$ into net $(\tilde{d}_{n:lM})$ and alternating

$(\tilde{d}_{n:lM})$ components as⁴⁷

$$\begin{aligned} d_{n:lM} &= \bar{d}_{n:lM} + \tilde{d}_{n:lM}; \\ \tilde{d}_{n:lM} &= \frac{1}{4}(2d_{n:lM} - d_{n-1:lM} - d_{n+1:lM}), \end{aligned} \quad (3.1)$$

and calculate the ratios $|\tilde{d}_{n:2M}/\tilde{d}_{n:1M}|$ (Fig. 4). These ratios are independent of the unit index n in any ground state and correspond to unity when three chains are proportionate in charge. $(++++)$ -M-CDW, bifurcating from $(+++)$ -M-CDW, is possibly of remarkable interchain charge polarization, where the interchain heterogeneity barometer $|\tilde{d}_{n:2M}/\tilde{d}_{n:1M}|$ goes almost down to 0.3, while $(-++)$ -M-CDW, discontinuously replacing $(+++)$ -M-CDW, is generally of moderate interchain charge polarization, where $|\tilde{d}_{n:2M}/\tilde{d}_{n:1M}|$ is not so far from unity. Then we may have an idea of describing the $(-++)$ -to- $(++++)$ -M-CDW transition in terms of weakly coupled CDW chains of Pt^{2+} and Pt^{4+} .

Figure 3(a) demonstrates that V_{MM}^{\times} and V_{MM}^{\perp} are the driving interactions for $(++++)$ -M-CDW and $(-++)$ -M-CDW, respectively. Under strong valence localization, their d -electron energies may be expressed as

$$\begin{aligned} \frac{E_{(++++)\text{-M-CDW}}}{N} &= 3\varepsilon_M - \frac{3\beta_M^2}{K_{MX}^{\parallel}} + \frac{3U_M}{2} \\ &\quad + 6V_{MM}^{\perp}, \end{aligned} \quad (3.2)$$

$$\begin{aligned} \frac{E_{(-++)\text{-M-CDW}}}{N} &= 3\varepsilon_M - \frac{3\beta_M^2}{K_{MX}^{\parallel}} + \frac{3U_M}{2} \\ &\quad + 2V_{MM}^{\perp} + 8V_{MM}^{\times}, \end{aligned} \quad (3.3)$$

which are balanced at $V_{MM}^{\perp} = 2V_{MM}^{\times}$ and are consistent with numerical findings in Fig. 3(a) to a certain extent. We can refine such an analytic consideration taking account of transfer effects. Decoupled chains, whether in $(++++)$ -M-CDW or in $(-++)$ -M-CDW, gain the

same hopping energy on the zeroth-order phase boundary $V_{MM}^\perp = 2V_{MM}^\times$. The interchain contact t_{MM}^\perp switched on contributes further stabilization energy to the $(-++)$ arrangement but is of no benefit to the $(+++)$ one. We obtain a correcter estimate of the phase boundary as

$$V_{MM}^\perp = 2V_{MM}^\times - \frac{(t_{MM}^\perp)^2}{4\beta_M^2/K_{MX}^\parallel - U_M + 4(V_{MM}^\parallel - V_{MM}^\times) + V_{MM}^\perp}, \quad (3.4)$$

provided $\sqrt{t_{MM}^\perp K_{MX}^\parallel} \ll \beta_M$, and it is indeed in excellent agreement with the numerical calculation. The standard parametrization of $V_{MM}^\perp = \sqrt{2}V_{MM}^\times$ applied to decoupled chains results in a $(+++)$ - M -CDW ground state. It is the advantage of interchain electron hopping that enables $(-++)$ - M -CDW to replace $(+++)$ - M -CDW. The close competition between $(+++)$ - M -CDW and $(-++)$ - M -CDW depends on electron-lattice couplings as well. With increasing β_M , $(-++)$ - M -CDW loses the advantage of interchain electron transfer $\propto (t_{MM}^\perp)^2$ and is again replaced by $(+++)$ - M -CDW, as is demonstrated in Fig. 3(b). In the moderate coupling region $(-++)$ - M -CDW generally plays the ground state, while with increasing electron-phonon interactions of the Peierls and/or Holstein types, $(+++)$ - M -CDW appears instead.

When we tune the band filling, we find M -CDW transitions between the $(+++)$ and $(++)$ types as well as those between the $(+++)$ and $(-++)$ types in the electron-doped region [Fig. 3(c)]. The collapse of the electron-hole symmetry results from the frustration-induced interchain charge polarization. Although $(+++)$ - M -CDW and $(-++)$ - M -CDW are born of the same representation $X E'(1) \otimes \tilde{S}^0 \otimes \tilde{T}^0$, their boundaries to $(+++)$ - M -CDW are different in character. The invariance groups of $(\pm++)$ - M -CDW and $(+++)$ - M -CDW are $\mathbf{C}_{2v}\mathbf{L}_2\mathbf{ST}$ and $\mathbf{D}_{3h}\mathbf{L}_2\mathbf{ST}$, respectively. Since the former is a subgroup of the latter, there may be a continuous transition of the second order between them, which is the case with any instability arising from PM of the full symmetry. $(+++)$ -to- $(++)$ - M -CDW transitions are indeed of the second order, whereas $(+++)$ -to- $(-++)$ - M -CDW transitions are of the first order. A continuous transition between distinct CDW states is unusual and has never been observed in any other MX compound. We thus wait eagerly for geometrically frustrated MX prisms to be fabricated.

Figure 3(c) stimulates another interest in platinum-halide nanotubes. There appears a quite interesting phase, $(0+-)$ - M -CDW, in the hole-doped region, which consists of Peierls-insulating dimerized chains and a paramagnetic regular chain. Figure 5 elucidates its energy structure, together with those of $(+++)$ - M -CDW and $(-++)$ - M -CDW. $(+++)$ - M -CDW and $(-++)$ - M -CDW are fully gapped, whereas $(0+-)$ - M -CDW is gapless and metallic. The metallic band is essentially composed of trivalent platinum ions [Fig. 5(c)], though there survives a finite contribution from those of trapped valence under the standard parametrization of intermediate

electron-lattice coupling. As a rule for $(0+-)$ - M -CDW, holes are doped into a single chain and the rest two remain half filled until the metallic chain is emptied. In $(-++)$ - M -CDW, on the other hand, the highest-lying filled band is made from a couple of Peierls-distorted chains in phase [Fig. 5(b)] and therefore, doped holes immediately eat into the two CDW chains. The two Peierls-distorted chains in $(0+-)$ - M -CDW are free from doped holes and thus remain stable, while two of the Peierls-distorted chains in $(-++)$ - M -CDW suffer from hole doping and are thus destabilized. Once the conduction electrons are removed out, $(0+-)$ - M -CDW is no more free from holes invading divalent platinum ions and suffers a rapid collapse. Thus and thus, there may be a re-entrant transition between $(-++)$ - M -CDW and $(0+-)$ - M -CDW. Figure 6 illustrates hole injection into $(-++)$ - M -CDW and $(0+-)$ - M -CDW under strong valence localization. Their d -electron energies are evaluated as

$$\begin{aligned} \frac{E_{(-++)-M\text{-CDW}}}{N} &= 3(1-\delta)\varepsilon_M + \frac{2+(2-3\delta)^2}{4}U_M \\ &+ \frac{(2-3\delta)^2}{2}V_{MM}^\perp + 4(2-3\delta)V_{MM}^\times \\ &- \frac{2+(2-3\delta)^2}{2}\frac{\beta_M^2}{K_{MX}^\parallel} \quad \left(0 \leq \delta \leq \frac{2}{3}\right), \end{aligned} \quad (3.5)$$

$$\begin{aligned} \frac{E_{(0+-)-M\text{-CDW}}}{N} &= 3(1-\delta)\varepsilon_M + \frac{4+(1-3\delta)^2}{4}U_M \\ &+ (1-3\delta)^2V_{MM}^\parallel + 2(1-3\delta)V_{MM}^\perp + 4(2-3\delta)V_{MM}^\times \\ &- \frac{2\beta_M^2}{K_{MX}^\parallel} \quad \left(0 \leq \delta \leq \frac{1}{3}\right), \end{aligned} \quad (3.6)$$

$$\begin{aligned} \frac{E_{(0+-)-M\text{-CDW}}}{N} &= 3(1-\delta)\varepsilon_M + \frac{9(1-\delta)^2}{4}U_M \\ &+ 9(1-\delta)^2V_{MM}^\times \\ &- \frac{9(1-\delta)^2}{2}\frac{\beta_M^2}{K_{MX}^\parallel} \quad \left(\frac{1}{3} \leq \delta \leq \frac{2}{3}\right), \end{aligned} \quad (3.7)$$

and are plotted in Fig. 6. In $(0+-)$ - M -CDW doped holes are distributed differently according as their density, defined as $3-4\nu \equiv \delta$, exceeds one third or not. That is why $(0+-)$ - M -CDW once replaces $(-++)$ - M -CDW but soon disappears with decreasing electron occupancy. The naivest estimates (3.5)-(3.7) succeed in predicting such a re-entrant transition, though they over-stabilize $(0+-)$ - M -CDW against $(-++)$ - M -CDW. The preceding transition point is well explained, but the succeeding one is harder to understand. It is likely that linear corrections of hopping energy to both $E_{(-++)-M\text{-CDW}}$ and $E_{(0+-)-M\text{-CDW}}$ should make their competition under doping much less intuitive.

IV. SUMMARY AND DISCUSSION

Platinum-halide triangular prisms are thus identified as frustrated Peierls-Hubbard nanotubes and are pro-

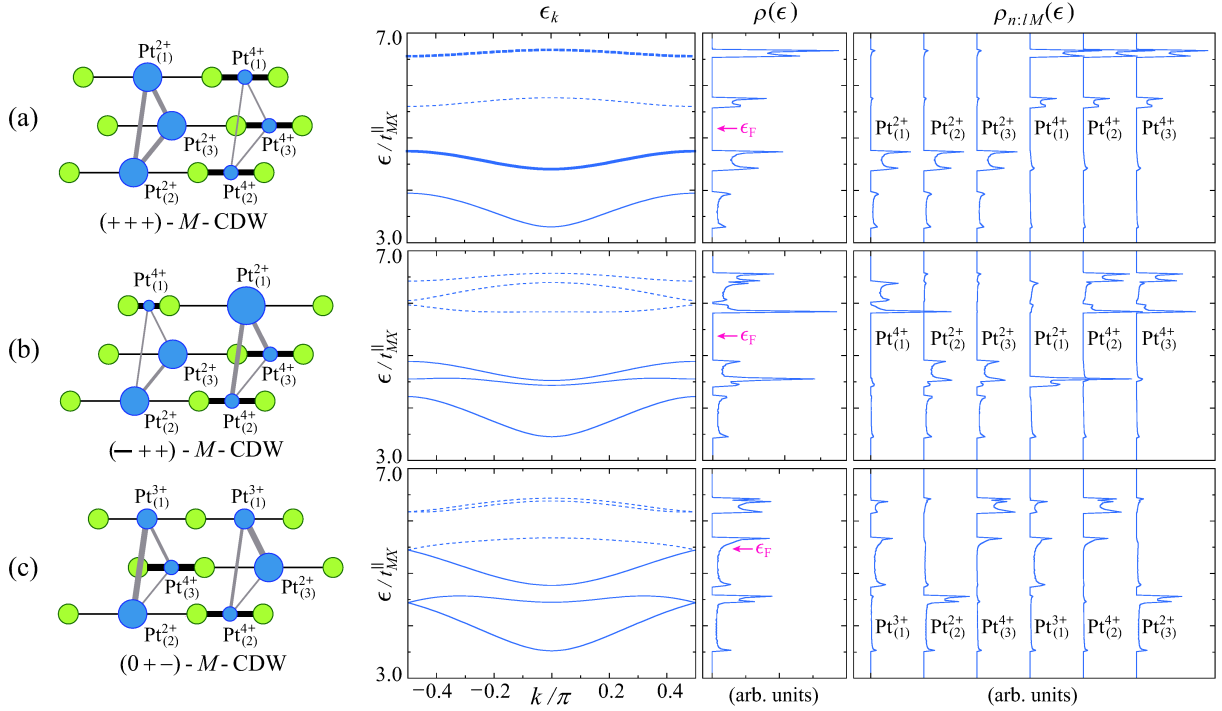


FIG. 5: (Color online) The single-particle energy dispersion relation ϵ_k and the local (total) density of states $\rho_{n:LA}(\epsilon)$ [$\rho(\epsilon) \equiv \sum_{n,l,A} \rho_{n:LA}(\epsilon)$] for $(+++)$ - M -CDW (a), $(-++)$ - M -CDW (b) and $(0+-)$ - M -CDW (c). We focus on the highest-lying six bands mainly of Pt character, where solid and dotted lines consist of occupied and vacant states, while thin and thick lines denote singly and doubly degenerate bands, respectively. ϵ_F indicates the Fermi level.

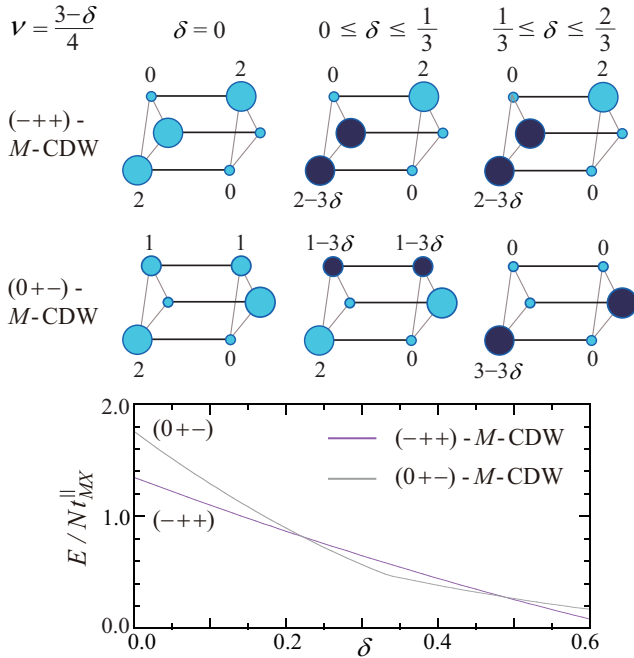


FIG. 6: (Color online) Electron occupancy of the Pt d_{z^2} orbitals as a function of the density of doped holes under strong valence localization on the assumption that the $X p_z$ orbitals remain fully filled and inactive. Energy estimates (3.5)-(3.7) are plotted as functions of $\delta \equiv 3 - 4\nu$, where ϵ_M is set equal to zero.

ductive of novel CDW states. Any structural instability is conditional and the homogeneous CDW state of D_{3h} symmetry is broken down into those of lower symmetry with increasing interchain transfer energy and/or varying electron occupancy. The geometric frustration unbalances three chains in charge and yields heterogeneous CDW states, which are possibly detectable by NMR chemical-shift⁴⁸ and X-ray scattering⁴⁹ measurements.

Electrochemical doping possibly causes successive phase transitions between totally valence-trapped and fully metallic states. We encounter both first- and second-order insulator-to-metal transitions under hole doping, whereas we find continuous transitions between distinct CDW states under electron doping. A stepwise increase in conductivity is expected of the discontinuous insulator-to-metal transition. It is the frustration-induced interchain charge polarization rather than the two-band modeling employed that breaks the electron-hole symmetry.

There is a possibility of structural instabilities of longer period existing under doping. Indeed we have extensively investigated solutions of $Q \neq \pi$, including incommensurate phases, but none of them competes in energy with those of $Q = \pi$ in the present modeling. Some examples are shown in Fig. 7. At $\nu = 2/3$ and $5/6$ the Pt d_{z^2} orbitals are effectively $1/3$ - and $2/3$ -filled, where formally commensurate, that is to say, cell-tripled, M -CDW states are found, while at $\nu = 7/10$ and $4/5$ the

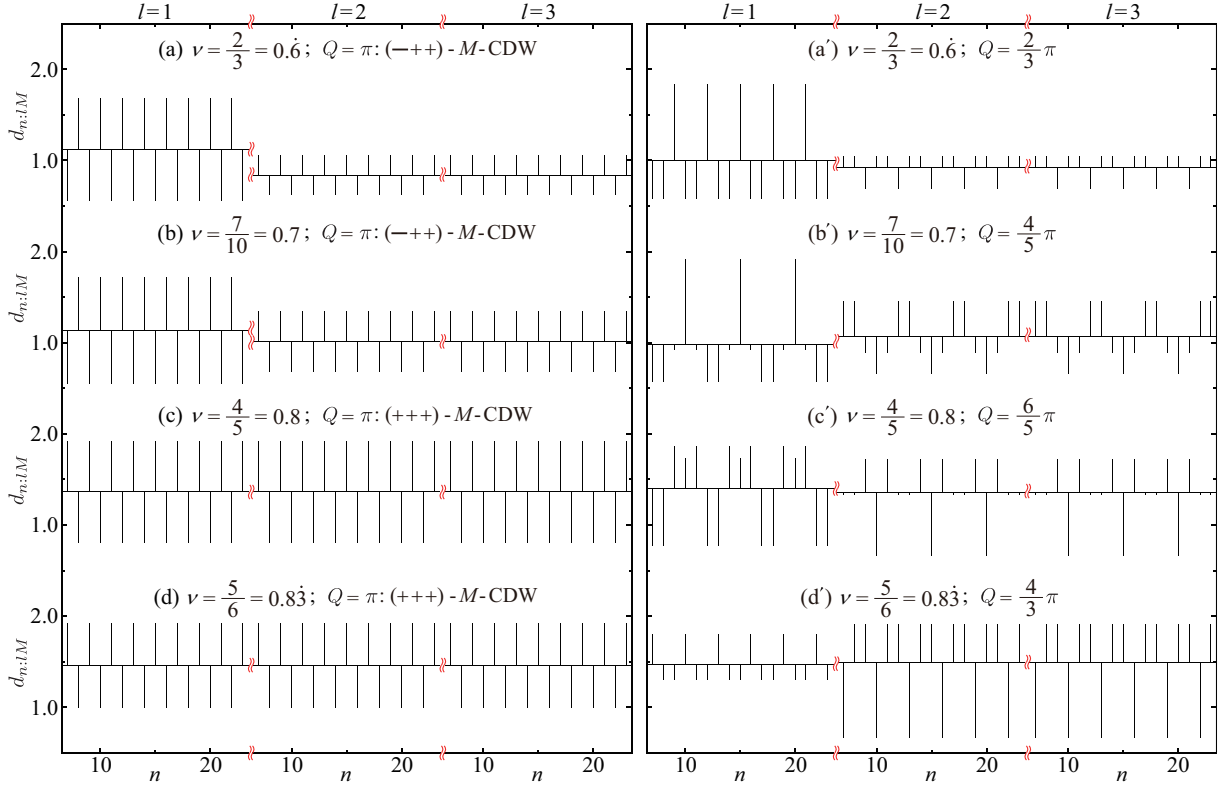


FIG. 7: (Color online) Metastable CDW states of $Q \neq \pi$ against the ground states, with $Q = \pi$, at various values of ν , where the local electron densities $d_{n,lM}$ are measured in comparison with the average occupancy of the relevant chain labeled l . Seventeen metal triangles are clipped out of the prism of $N = 300$.

Pt d_{z^2} orbitals are effectively 2/5- and 3/5-filled, where subharmonic, namely, cell-quintupled, M -CDW states are found. Trimerized CDW solutions are available at $0.646 \lesssim \nu \lesssim 0.694$ and $0.805 \lesssim \nu \lesssim 0.847$, whereas pentamerized ones are detectable at $0.691 \lesssim \nu \lesssim 0.733$ and $0.783 \lesssim \nu \lesssim 0.833$, but they are never stabilized into the ground state under the standard parametrization. With increasing β , however, they closely compete in energy with dimerized CDW solutions and finally become preferable in general. In the cases of $\nu = 2/3$ and $5/6$, the transition points are estimated at $\beta/\sqrt{t_{MX}^{\parallel} K_{MX}^{\parallel}} \simeq 0.705$ and 0.814 , respectively, while in the cases of $\nu = 7/10$ and $4/5$, they turn out $\beta/\sqrt{t_{MX}^{\parallel} K_{MX}^{\parallel}} \simeq 0.765$ and 0.855 , respectively, all of which may be too large to be realized in available platinum halides. It was predicted for a single MX chain that incommensurate ground states should

appear even at $3/4$ filling provided the site-diagonal electron-lattice coupling is sufficiently strong,⁵⁰ but they are not yet observed experimentally.

There is an attempt at fabricating a platinum-bromide triple-chain compound.⁵¹ Substitution of platinum ions with nickel ions should lead to stronger correlations between d electrons and might result in novel spin arrangements. We hope our calculations will stimulate further chemical explorations of tubed MX compounds.

Acknowledgments

We are grateful to K. Otubo and H. Kitagawa for valuable information on their extensive chemical explorations. This work was supported by the Ministry of Education, Culture, Sports, Science and Technology of Japan.

¹ S. Iijima: Nature **354** (1991) 56.

² T. W. Ebbesen and P. M. Ajayan: Nature **358** (1992) 220.

³ J. Kong, H. T. Soh, A. M. Cassell, C. F. Quate and H. Dai: Nature **395** (1998) 878.

⁴ W. Clauss, D. J. Bergeron and A. T. Johnson: Phys. Rev. B **58** (1998) R4266.

⁵ R. Saito, M. Fujita, G. Dresselhaus and M. S. Dresselhaus:

Appl. Phys. Lett. **60** (1992) 2204.

⁶ R. Saito, M. Fujita, G. Dresselhaus and M. S. Dresselhaus: Phys. Rev. B **46** (1992) 1804.

⁷ P. Millet, J. Y. Henry, F. Mila and J. Galy: J. Solid State Chem. **147** (1999) 676.

⁸ G. Seeber, P. Kögerler, B. M. Kariuki and L. Cronin: Chem. Commun. **2004** (2004) 1580.

- ⁹ K. Otsubo, Y. Wakabayashi, J. Ohara, S. Yamamoto, H. Matsuzaki, H. Okamoto and H. Kitagawa: unpublished.
- ¹⁰ J. Ohara and S. Yamamoto: *Europhys. Lett.* **87** (2009) 17006.
- ¹¹ A. Mishima and K. Nasu: *Phys. Rev. B* **39** (1989) 5758.
- ¹² A. Mishima and K. Nasu: *Phys. Rev. B* **39** (1989) 5763.
- ¹³ J. T. Gammel, A. Saxena, I. Batistić, A. R. Bishop, and S. R. Phillpot: *Phys. Rev. B* **45** (1992) 6408.
- ¹⁴ S. M. Weber-Milbrodt, J. T. Gammel, A. R. Bishop and E. Y. Loh, Jr.: *Phys. Rev. B* **45** (1992) 6435.
- ¹⁵ H. Okamoto and M. Yamashita: *Bull. Chem. Soc. Jpn.* **71** (1998) 2023.
- ¹⁶ B. M. Craven and D. Hall: *Acta Cryst.* **14** (1961) 475.
- ¹⁷ H. Toftlund and O. Simonsen: *Inorg. Chem.* **23** (1984) 4261.
- ¹⁸ K. Toriumi, Y. Wada, T. Mitani, S. Bandow, M. Yamashita, and Y. Fujii: *J. Am. Chem. Soc.* **111** (1989) 2341.
- ¹⁹ K. Iwano: *Phys. Rev. B* **70** (2004) 241102(R).
- ²⁰ H. Matsuzaki, M. Yamashita and H. Okamoto: *J. Phys. Soc. Jpn.* **75** (2006) 123701.
- ²¹ K. Marumoto, H. Tanaka, S. Kuroda, T. Manabe and M. Yamashita: *Phys. Rev. B* **60** (1999) 7699.
- ²² H. Matsuzaki, K. Iwano, T. Aizawa, M. Ono, H. Kishida, M. Yamashita and H. Okamoto: *Phys. Rev. B* **70** (2004) 035204.
- ²³ S. Yamamoto: *Phys. Rev. B* **63** (2001) 125124.
- ²⁴ M. Kuwabara and K. Yonemitsu: *J. Mater. Chem.* **11** (2001) 2163.
- ²⁵ M. Kurmoo and R. J. H. Clark: *Inorg. Chem.* **24** (1985) 4420.
- ²⁶ B. I. Swanson, M. A. Stroud, S. D. Conradson and M. H. Zietlow: *Solid State Commun.* **65** (1988) 1405.
- ²⁷ S. Yamamoto: *Phys. Rev. B* **64** (2001) 140102(R).
- ²⁸ S. Yamamoto: *J. Phys. Chem. Solids* **63** (2002) 1489.
- ²⁹ H. Matsuzaki, T. Matsuoaka, H. Kishida, K. Takizawa, H. Miyasaka, K. Sugiura, M. Yamashita and H. Okamoto: *Phys. Rev. Lett.* **90** (2003) 046401.
- ³⁰ K. Yonemitsu and N. Miyashita: *Phys. Rev. B* **68** (2003) 075113.
- ³¹ C. Bellitto, A. Flamini, L. Gastaldi and L. Scaramuzza: *Inorg. Chem.* **22** (1983) 444.
- ³² H. Kitagawa, N. Onodera, T. Sonoyama, M. Yamamoto, T. Fukawa, T. Mitani, M. Seto and Y. Maeda: *J. Am. Chem. Soc.* **121** (1999) 10068.
- ³³ S. Yamamoto: *J. Phys. Soc. Jpn.* **70** (2001) 1198.
- ³⁴ D. Kawakami, M. Yamashita, S. Matsunaga, S. Takaishi, T. Kajiwara, H. Miyasaka, K. Sugiura, H. Matsuzaki and H. Okamoto: *Angew. Chem.* **118** (2006) 7372.
- ³⁵ A. Kobayashi and H. Kitagawa: *J. Am. Chem. Soc.* **128** (2006) 12066.
- ³⁶ K. Funase and S. Yamamoto: *J. Phys. Soc. Jpn.* **75** (2006) 044717.
- ³⁷ K. Iwano and Y. Shimoi: *J. Phys. Soc. Jpn.* **76** (2007) 063708.
- ³⁸ S. Yamamoto and J. Ohara: *Phys. Rev. B* **76** (2007) 235116.
- ³⁹ S. Yamamoto and J. Ohara: *J. Mater. Sci.: Mater. Electron.* **20** (2009) S367.
- ⁴⁰ A. Nakanishi, M. Hamada, A. Goto and M. Ozaki: *Prog. Theor. Phys.* **118** (2007) 413.
- ⁴¹ M. Hamada, A. Nakanishi, A. Goto and M. Ozaki: *Prog. Theor. Phys.* **121** (2009) 391.
- ⁴² S. Yamamoto and M. Ozaki: *Solid State Commun.* **83** (1992) 329.
- ⁴³ S. Yamamoto and M. Ozaki: *Solid State Commun.* **83** (1992) 335.
- ⁴⁴ M. Golubitsky, I. Stewart and D. G. Schaeffer: *Singularity and Groups in Bifurcation Theory* (Springer-Verlag, Berlin, 1985) Vol. II, p. 83.
- ⁴⁵ D. Baeriswyl and A. R. Bishop: *J. Phys.: Condens. Matter* **21** (1988) 339.
- ⁴⁶ S. Yamamoto: *Phys. Lett. A* **247** (1998) 422.
- ⁴⁷ S. Yamamoto: *Phys. Rev. B* **66** (2002) 165113.
- ⁴⁸ N. Kimura, H. Ohki, R. Ikeda and M. Yamashita: *Chem. Phys. Lett.* **220** (1994) 40.
- ⁴⁹ Y. Wakabayashi, A. Kobayashi, H. Sawa, H. Ohsumi, N. Ikeda and H. Kitagawa: *J. Am. Chem. Soc.* **128** (2006) 6676.
- ⁵⁰ I. Batistić, J. T. Gammel and A. R. Bishop: *Phys. Rev. B* **44** (1991) 13228.
- ⁵¹ K. Otsubo and H. Kitagawa: private communication.